THE JOURNAL OF PHYSICAL CHEMISTRY C

Article

pubs.acs.org/JPCC

Molecular Dynamics Simulations of Ion-Bombarded Graphene

Edson P. Bellido[†,‡] and Jorge M. Seminario*[,†,‡,§]

[†]Department of Chemical Engineering, [‡]Materials Science and Engineering Graduate Program, and [§]Department of Electrical and Computer Engineering, Texas A&M University, College Station, Texas 77843, United States

ABSTRACT: Using molecular dynamics simulations and a hybrid Tersoff-ZBL potential, the effects of irradiating graphene with a carbon ion at several positions and several energies from 0.1 eV to 100 keV are studied. The simulations show four types of processes: absorption, reflection, transmission, and vacancy formation. At energies below 10 eV, the dominant process is reflection; between 10 and 100 eV, it is absorption; and between 100 eV and 100 keV, the dominant process is transmission. Vacancy formation is a low-probability process that takes place at energies above 30 eV. Three types of defects are found: adatom, single vacancy, and 5−8−5 defect formed from a double-vacancy defect. The simulations provide a fundamental understanding of the graphene carbon bombardment and the parameters to develop graphene devices by controlling defect formation.

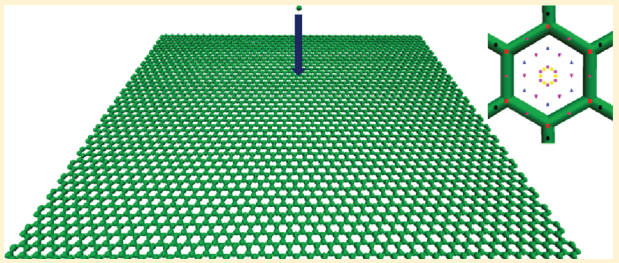

INTRODUCTION

Graphene is a material of high technological importance due to its unique electrical and mechanical properties and the rich physics phenomena observed in several studies.[1−8] Graphene is a promising material used in several electronic applications such as transistors,[9,10] transparent electrodes,[11] and sensors;[12−14] most applications require control over the electrical and structural properties. Functionalization is one method of modifying the band structure of graphene; however, surface functionalization is not easily achieved and generally occurs at the graphene edges.[15] Another method of tuning the graphene electronic properties is by defect formation.[16] Defects are intrinsic in graphene production; however, defects can also be created intentionally by ion bombardment and scanning probe lithography.[17,18] Scanning probe lithography techniques can be used to modify graphene structures with high precision, but the techniques are not adequate for mass production. On the other hand, ion beams can be scanned over graphene faster than mechanical tips, with the advancements in ion beam technology allowing the spot size to be as small as a few nanometers in diameter. Recently, Garaj et al.[19] synthesized graphene film with controllable thickness by ion implantation of carbon atoms on nickel substrates; after implantation, the samples were heated and the carbon atoms diffused to the surface forming graphene. A convenient methodology for mass production of graphene devices would be to use the same process from the material synthesis to the final device fabrication. The next step for the graphene circuit development is to control the electronic properties by defect formation using carbon atoms for the ion bombardment of graphene. In this study, molecular dynamics (MD) on the bombardment of graphene with carbon atoms in a variety of sites and at several shooting energies were simulated. The physics behind the ion bombardment of graphene with carbon atoms will provide models with their parameters to develop a precise experimental lithography methodology for controlled defect production, which will lead ultimately to graphene integrated device fabrication allowing the full development of molecular and nanoelectronics. Models can be designed based on the physics behind ion bombardment of graphene with carbon atoms using their parameters to develop precise experimental lithography methods for controlled defect production, which will ultimately lead to graphene-integrated device fabrication leading to the full development of molecular and nanoelectronics.[20]

METHODOLOGY

We perform classical MD simulations using the LAMMPS[21] program. The interaction between atoms

$$V = \frac{1}{2}\sum_{i}\sum_{j\neq i} V_{ij} \tag{1}$$

is modeled with a three-body Tersoff potential,[22−25] V_{ij}, which incorporates the dependence of bond order on the local environment. V_{ij} includes a short-distance term based on a Ziegler−Biersack−Littmark (ZBL) potential,[26] which is a screening potential for repulsion at very small interatomic distances.

$$V_{ij} = (1 - f_F(r_{ij}))V_{ij}^{ZBL} + f_F(r_{ij})V_{ij}^{Tersoff} \tag{2}$$

where the f_F term

$$f_F(r_{ij}) = \frac{1}{1 + \exp(-A_F(r_{ij} - r_C))} \tag{3}$$

Received: August 21, 2011
Revised: January 14, 2012
Published: January 16, 2012

is a Fermi-like function that smoothly connects the Tersoff and the ZBL potentials. A_F and r_C are control parameters of the function shape. The ZBL potential has two factors

$$V_{ij}^{ZBL} = \frac{1}{4\pi\varepsilon_0}\frac{Z_i Z_j e^2}{r_{ij}}\varnothing\left(\frac{r_{ij}}{a}\right) \quad (4)$$

The first factor is the Coulombic potential, where Z_i and Z_j are the atomic numbers of the two atoms, e is the electron charge, and ε_0 is the vacuum permittivity. The second term, $\varnothing$, is a screening function given by

$$\varnothing(x) = 0.1818e^{-3.2x} + 0.5099e^{-0.9423x} + 0.2802 e^{-0.4029x} + 0.02817e^{-0.2016x} \quad (5)$$

with

$$a = \frac{0.8854a_0}{Z_i^{0.23} + Z_j^{0.23}} \quad (6)$$

where a_0 is the Bohr radius and the a function is accurate for small separations (<1 Å). The ZBL potential, also known as the universal repulsive potential, is the most widely used analytical potential to describe collisions.[27−29] The accuracy of the ZBL potential has been tested comparing values of screening function of ZBL to ab initio methods (density functional theory (DFT) and Hartree−Fock), and it was observed that there is a difference of <0.7% for several pairs of atoms including the C−C interaction.[29]

The Tersoff potential has four terms

$$V_{ij}^{Tersoff} = f_C(r_{ij})[f_R(r_{ij}) + b_{ij}f_A(r_{ij})] \quad (7)$$

where f_C is a smooth cutoff function to limit the range of the potential and goes from 0 to 1 in a small range D around R.

$$f_C(r) = \begin{cases} 1 & ; r < R - D \\ \frac{1}{2} - \frac{1}{2}\sin\left(\frac{\pi}{2}\frac{r-R}{D}\right) & ; R - D < r < R + D \\ 0 & ; r > R + D \end{cases} \quad (8)$$

The functions

$$f_R(r) = Ae^{-\lambda_1 r} \quad (9)$$

and

$$f_A(r) = -Be^{-\lambda_2 r} \quad (10)$$

are repulsive and attractive Morse-like potentials, respectively. The b_{ij} functions are measures of bond order

$$b_{ij} = (1 + \beta^n\zeta_{ij}^n)^{-1/2n} \quad (11)$$

and depends on the ζ function

$$\zeta_{ij} = \sum_{k\neq ij} f_C(r_{ik})g(\theta_{ijk})\exp(-[\lambda_3^3(r_{ij} - r_{ik})^m]) \quad (12)$$

where the $g(\theta)$ function is defined as

$$g(\theta) = \gamma_{ijk}\left(1 + \frac{c^2}{d^2} - \frac{c^2}{|d^2 + (\cos\theta - h)^2|}\right) \quad (13)$$

where θ represents the angle between bonds ij and ik and γ_{ijk} is a parameter used to strengthen or weaken bonds between different types of atoms. In the simulations conducted, γ_{ijk} has a value of one because we have only one type of atom. Parameters chosen to fit the cohesive energy, bulk modulus, and lattice constant of several polytypes of carbon are m, γ, λ_3, c, d, h, n, and β, depending on their coordination number.[23,24] Parameters used in the simulations are shown in Table 1.

Table 1. Parameters of the Ion Bombardment Simulations

parameter	value	parameter	value
m	3	B	346.7 eV
γ	1	R	1.95 Å
λ_3	0.0 Å^{-1}	D	0.15 Å
c	38049	λ_1	3.4879 Å^{-1}
d	4.3484	A	1393.6 eV
h	−0.57058	Z	6
n	0.72751	r_C	0.95 Å
β	1.5724×10^{-7}	A_F	14
λ_2	2.2119 Å^{-1}		

The modeled system is a 10 × 10 nm^2 graphene sheet centered at the origin of coordinates, laying on the x-y plane; a carbon atom is positioned 3 nm from the graphene in the z axis, as shown in Figure 1. Two opposite ends of the graphene are

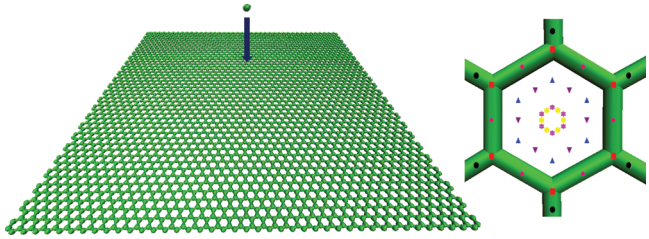

Figure 1. Simulated system, where a carbon atom hits a suspended graphene sheet. The inset shows the selected positions where the carbon ion hits the graphene. The symmetric atoms are color-coded: black ellipses (group a), red squares (group b), pink diamonds (group c), blue triangles (group d), purple down triangles (group e), magenta stars (group f), and yellow hexagons (group g).

fixed to simulate a suspended system. The simulations are carried out with a time step of 0.05 fs for energies between 0.1 and 100 eV and 0.01 fs for energies between 100 eV and 100 keV. The time steps are designated to ensure that there are enough steps during atom interactions that occur within the potential cutoff length of 2.1 Å. After minimization, the simulations follow a temperature ramp with a Berendsen thermostat[30] from 10 to 300 K and a damping time of 100 fs. Then, the system is kept at 300 K with 100 fs damping time until the system reaches equilibrium. Finally, an NVE ensemble is set for the rest of the simulations where the ion bombardment occurred. A velocity is imposed in the $-z$ direction to the shooter carbon atom according to a range of selected energy values.

A neutral carbon atom is considered for the bombardment simulations; named hereafter ion, despite the fact that the atom had no explicit net charge.

The ion charge is not considered because if the bombardment were performed with charged atoms then the charge of the ion would have been neutralized on the surface by charge exchange, considering that the electron movement is at least

dx.doi.org/10.1021/jp208049t | J. Phys. Chem. C 2012, 116, 4044−4049

three orders of magnitude faster than the nuclei. Therefore, the dynamics of the carbon ion is assumed to be similar to that of the neutral carbon atom within the Oppenheimer approximation.[27,31] This argument is even strengthened by the fact that in the experiments the charge accumulation is prevented by grounding the bombarded sample; therefore, the charge each ion carries is always neutralized when it strikes the target.[32]

The specified initial position of the ion is perpendicular to where the ion hits the graphene, which is selected to have six symmetric points for each initial position, as shown in the inset of Figure 1. Every color represents a group of symmetric points, and they will be referred to as follows: black ellipses (a), red squares (b), pink diamonds (c), blue triangles (d), purple down triangles (e), magenta stars (f), and yellow hexagons (g).

After the MD simulations, the atomic structure of the defects formed by ion bombardment is separated from the complete graphene structure, leaving the defect at the center of the separated piece of graphene structure, which is used later to perform ab initio calculations. The dangling carbon bonds in the borders are completed with hydrogen atoms to avoid deformations due to reactive sites; on the average, the separated structures contain ~90 atoms. Then, the separated graphene structure is optimized by ab initio DFT using the B3PW91 hybrid functional[33,34] and the 6-31G(d) basis sets.[35] Convergences are set within a threshold on the density matrix of 10^{-6} and 10^{-8} for the root-mean-square and the maximum density matrix error between iterations, respectively. The geometry optimizations are followed by a second derivative calculation to determine the existence of a local minimum. The MD[36,37] and ab initio[38−40] approaches have been successfully used in the past.

RESULTS AND ANALYSIS

The interactions between the ion and the graphene sheet in the bombardment simulations present four cases: reflection, absorption, defect formation (damage), and transmission. These four types of interactions depict a clear dependence on the ion incident energy, as shown in Figure 2. At energies below

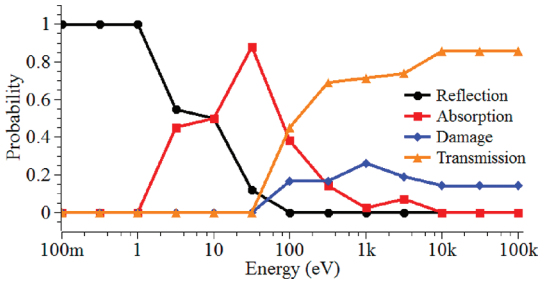

Figure 2. Probability of occurrence versus kinetic energy of the incident atom for reflection, absorption, damage, and transmission events.

1 eV, all of the incident ions are reflected. At energies above 1 eV, the reflection probability decreases until the energy reaches 100 eV, where no ions are reflected anymore. At low energies, the ions cannot overcome the barrier of the Tersoff bond-order potential and are reflected; as the energy of the ion increases, the probability of overcoming this barrier increases, and fewer ions are reflected. For graphene, this potential barrier is representing the π electrons that form a delocalized orbital over the surface of graphene, creating a repulsion of the incident ions.[13] At 1 eV, the incident atom has enough energy to overcome the electrostatic repulsion and absorption of the ion by the graphene surface takes place; the incident carbon atom forms a covalent bond with a nearby atom. At 30 eV, the absorption process becomes dominant. At energies greater than 100 eV, the absorption probability decreases, approaching zero at 10 keV. Defect formation is a low probability process that starts at 100 eV, reaching its maximum value at 1 keV with a probability of 0.26 and eventually reaching a constant probability of 0.14 at energies greater than 10 keV. During this process, two types of defects are created: single vacancy and double vacancy. At high energies, the dominant interaction is transmission; the probability increases smoothly between 30 eV and 10 keV, where it becomes constant with a value of 0.86.

The probabilities shown in Figure 2 also have a dependence on the site where the ion hits the graphene sheet. Considering that the temperature of the graphene sheet is at 300 K, it is clear that the lattice vibration plays an important role in the simulation results. The probabilities of Figure 2 can be related to the type of event that occurs when we have a group of symmetric points where the ion impacts the graphene. Figure 3 displays the types of processes for each impact position at several energies. In a group of points, not all positions show the same type of process. Figure 3 also shows that at energies below 1 eV the type of event is independent of the position and energy; all the incident ions are reflected. For 10 keV and above, the process method is independent of the ion kinetic energy, but there are two cases depending on the impact position. The ion that hits the top of a carbon atom produces a defect; however, in the other cases, the atoms are transmitted.

At intermediate energies, from 3 eV to 3 keV, there are a variety of dynamic processes depending on position and energy. At 3 eV, the ions that impact near the graphene carbon atom (groups a, b, and d) form a bond; the bond formation indicates that attractive interactions between carbon atoms contribute to overcoming the electrostatic repulsion and promotes bond formation. At 10 eV, the energy of the incident ion overcomes the electrostatic repulsion due to the π electrons (potential barrier) and a bond formation takes place; however, when the impacted position is closer to a carbon atom, the nuclear repulsion due to the direct impact prevents the bond formation and the ion is reflected.

At 30 eV, absorption is the preferred process at most of the impact positions. For ions in group "a", nuclear repulsion prevents the formation of a bond and the atom is reflected; however, the reflected ion interacts with neighboring atoms and forms a bond. For group "b" atoms, the preferred event is reflection, suggesting that the nuclear repulsion is due to the direct impact preventing the bond formation and reflecting the ion. For atoms in group "c", the ion passes through the graphene sheet but is stopped after crossing and forms a bond at the back of the graphene. For atoms in groups "d", "e", "f", and "g", two cases exist without dependence of position. The first case is similar to group "c" with a bond formation at the back of the graphene. In the second case, the incident ion removes a carbon atom; the removed carbon atom then forms a bond with a nearby atom.

At 100 eV, some of the ions are transmitted. In groups "f" and "g", all atoms are transmitted, and most of the atoms are transmitted for group "e"; these events suggest that the ions have enough energy to overcome the electrostatic repulsion and that the attractive interaction between the atoms is not enough to promote bond formation and the ions can pass through the graphene sheet because there is not a collision event. Atoms in

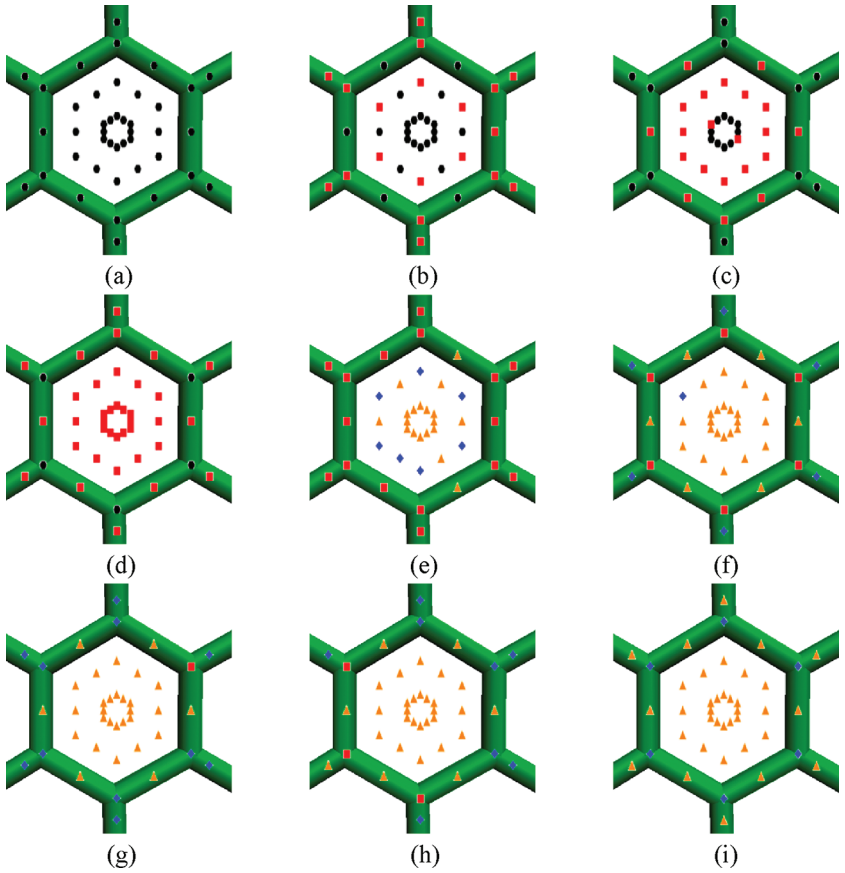

Figure 3. Impact positions at 0.1, 0.3, and 1 eV (a); 3 eV (b); 10 eV (c); 30 eV (d); 100 eV (e); 300 eV (f); 1 keV (g); 3 keV (h); and 10, 31, and 100 keV (i). The type of interaction is color-coded: black (reflection), red (absorption), blue (damage), and orang e(transmission).

group "d" exhibit a strong interaction between ions and carbon atoms; this suggests that the repulsive interaction is nuclear in origin. Because of the repulsion interaction, a carbon atom is removed and a defect is formed. In the case of groups "a" and "b" and most of group "c", there is a new type of process where the incident ion removes one carbon atom and occupies the place of the missing atom (removal/absorption). For groups "a" and "c", the atomic interaction is similar to the case of group "d", where the nuclear repulsion removes the carbon atom. For group "b", the interaction is considered to be a direct collision between the ion and the carbon atom; after the removal of the carbon atom, the interaction between the incident ion and the neighboring atoms promotes bond formation. It should be noted that for the sake of analysis we consider this process to be absorption because the incident ion is bonded to the graphene structure.

At 300 eV, most of the events are transmission; for groups "c" and "d", the repulsive interactions with the carbon atoms disturb the graphene lattice in some cases with temporary broken bonds. However, the incoming ion interacts repulsively with the graphene sheet for a smaller amount of time than for the case of 100 eV; the ion is finally transmitted in most of the cases. For group "a", the repulsive interaction is still strong enough to generate a defect. For group "b", the direct collision produces a removal/absorption event.

Between 1 and 3 keV, most of the atoms are transmitted. However, for group "a", there is still a strong repulsive interaction that promotes defect formation. For group "b", the direct collision produces removal/absorption events in some cases and defect formation in others. In this range of energies, we observe the formation of double vacancy defects. Finally, for energies 10 keV and higher, almost all atoms are transmitted except for group "b", where the direct collision forms single- and double-vacancy defects.

Another factor to be analyzed in the ion−graphene interactions is the kinetic energy of the ion before and after the interaction with the graphene. The ratio of the incident kinetic energy to the energy after the ion interacts with the graphene is a measurement of the degree of interaction and the amount of energy gained by the graphene structure. Figure 4

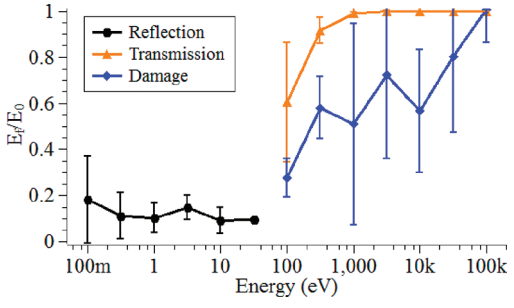

Figure 4. Ratio between the kinetic energy of the carbon ion after and before hitting the graphene for reflection, transmission and damage.

shows the ratio of kinetic energy after and before the impact for reflection, transmission, and damage. From these curves, we can see that for the case of reflection, the interaction between the ion and the graphene is stronger and the ion loses most of its energy. This effect can be attributed to the ion−carbon

dx.doi.org/10.1021/jp208049t | J. Phys. Chem. C 2012, 116, 4044−4049

interaction time; at low energies, as in the case of the reflection events, the interaction time is long enough to allow local energy equilibration and the graphene gains energy from the ion. For the case of reflection, as the ion energy increases, the penetration depth increases, increasing at the same time as the atomic attractive interaction. This effect promotes energy exchange especially for the hitting positions not close enough to the carbon atoms that can produce nuclear repulsion. For the transmission case, Figure 4 shows that as the ion energy increases, the energy exchange between graphene and the ion decreases (ion kinetic energy after interaction increases) due to the reduction in the ion−carbon interaction time, leaving graphene almost unperturbed at high energies. When a defect is formed, the same trend as in transmission is observed; as the energy increases, the energy exchange decreases; similarly, this behavior can be attributed to the interaction time between the ion and carbon atoms in the graphene sheet. The impact position also plays a role; the closer the ion collides with a carbon atom, the higher the exchange energy (the lower the ion kinetic energy).

In the simulations, three types of defects are obtained: one formed by the absorption process and two formed by vacancy formation. After the molecular dynamic simulations, the atomic structure of the defects is optimized using DFT to get a stable structure with a more precise quantum-based method. For the case of absorption, two structures from the MD simulation are developed; however, after the DFT optimization, both structures converge to the same geometry, as shown in Figure 5a. This structure, called adatom, has already been observed

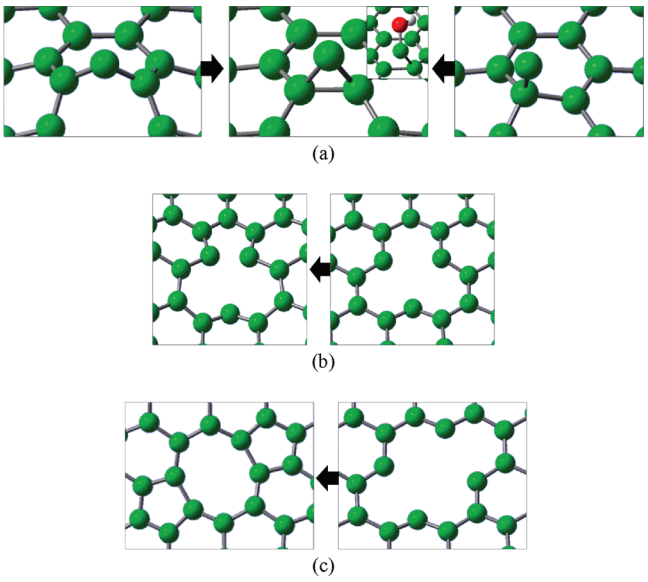

Figure 5. (a) Adatom defect after ab initio optimization (middle) of MD structures (left and right). The inset is a hydroxyl functionalization formed from the adatom defect. (b) Single vacancy defect and (c) double vacancy 5−8−5 defect after the ab initio optimization (left) of MD structures (right). The threshold distance for drawing a bond is 1.6324 Å.

experimentally, confirming that it is a stable defect of graphene under high-vacuum conditions.[41]

To test the stability of the adatom defect in a nonvacuum environment, the graphene sheet is optimized with an adatom defect in close proximity of a hydroxyl group, and a covalent bond is formed between the carbon atom of the adatom defect and the oxygen atom of the hydroxyl group. Finally, a functionalized graphene sheet is obtained; the reaction is energetically favorable with formation energy of 145 kcal/mol. When the carbon atoms are removed, two cases arise: single and double vacancy formation. In the single vacancy, as shown in Figure 5b, after the ab initio optimization, the distance between two of the carbon atoms closer to the vacancy decreases from 2.63 to 1.69 Å. For double vacancy, Figure 5c shows that the defect is reconstructed after optimization, forming two heptagons and one octagon (5−8−5 defect). These two types of defects formed by vacancies have also been observed experimentally,[41] confirming the accuracy of our calculations.

CONCLUSIONS

The carbon ion bombardment of graphene is simulated at several energies between 0.1 eV and 100 keV. Four types of interactions are observed: reflection, absorption, transmission, and vacancy formation. Reflection is the dominant process at low energies and is principally caused by the repulsive interaction of the carbon ion and the π electrons on the graphene sheet. At energies above 1 eV, the carbon ions have enough energy to overcome the π electron repulsion, and there is an absorption process, which is the dominant process between 10 and 100 eV. From the absorption events, adatom defects are formed. The final defect structures are optimized by ab initio calculations. Transmission events are observed at energies above 30 eV, becoming the dominant interaction after 100 eV. Vacancy formation is observed at energies above 30 eV and is a low-probability process with a constant probability of 0.14 at energies above 10 keV. From this process, single vacancies and double vacancies are obtained. From the double vacancies, a 5−8−5 defect is obtained after optimization using ab initio calculations. This work provides the analysis and physical parameters to understand the carbon ion bombardment of graphene necessary to develop a lithography method for controlled defect formation that will be a tool in the development of integrated graphene-based device fabrication.

AUTHOR INFORMATION

Notes

The authors declare no competing financial interest.

ACKNOWLEDGMENTS

We thank Akash Pernankil for a thorough reading of this manuscript. We acknowledge financial support from the U.S. Defense Threat Reduction Agency DTRA through the U.S. Army Research Office, projects no. W91NF-06-1-0231, ARO/DURINT project no. W91NF-07-1-0199, and ARO/MURI project no. W911NF-11-1-0024.

REFERENCES

(1) Novoselov, K. S.; Geim, A. K.; Morozov, S. V.; Jiang, D.; Zhang, Y.; Dubonos, S. V.; Grigorieva, I. V.; Firsov, A. A. *Science* **2004**, *306*, 666−669.

(2) Novoselov, K. S.; Jiang, D.; Schedin, F.; Booth, T. J.; Khotkevich, V. V.; Morozov, S. V.; Geim, A. K. *Proc. Natl. Acad. Sci. U.S.A.* **2005**, *102*, 10451−10453.

(3) Novoselov, K. S.; Geim, A. K.; Morozov, S. V.; Jiang, D.; Katsnelson, M. I.; Grigorieva, I. V.; Dubonos, S. V.; Firsov, A. A. *Nature* **2005**, *438*, 197−200.

(4) Novoselov, K. S.; McCann, E.; Morozov, S. V.; Fal'ko, V. I.; Katsnelson, M. I.; Zeitler, U.; Jiang, D.; Schedin, F.; Geim, A. K. *Nat. Phys.* **2006**, *2*, 177−180.
(5) Hill, E. W.; Geim, A. K.; Novoselov, K.; Schedin, F.; Blake, P. *IEEE Trans. Magn.* **2006**, *42*, 2694−2696.
(6) Lee, C.; Wei, X. D.; Kysar, J. W.; Hone, J. *Science* **2008**, *321*, 385−388.
(7) Stankovich, S.; Dikin, D. A.; Dommett, G. H. B.; Kohlhaas, K. M.; Zimney, E. J.; Stach, E. A.; Piner, R. D.; Nguyen, S. T.; Ruoff, R. S. *Nature* **2006**, *442*, 282−286.
(8) Bellido, E. P.; Seminario, J. M. *J. Phys. Chem. C* **2010**, *114*, 22472−22477.
(9) Lemme, M. C.; Echtermeyer, T. J.; Baus, M.; Kurz, H. *IEEE Electron Device Lett.* **2007**, *28*, 282−284.
(10) Lin, Y. M.; Jenkins, K. A.; Valdes-Garcia, A.; Small, J. P.; Farmer, D. B.; Avouris, P. *Nano Lett.* **2009**, *9*, 422−426.
(11) Bae, S.; Kim, H.; Lee, Y.; Xu, X. F.; Park, J. S.; Zheng, Y.; Balakrishnan, J.; Lei, T.; Kim, H. R.; Song, Y. I.; et al. *Nat. Nanotechnol.* **2010**, *5*, 574−578.
(12) Rangel, N. L.; Seminario, J. M. *J. Phys. B: At. Mol. Phys.* **2010**, *43*, 115101-1−115101-5.
(13) Rangel, N. L.; Seminario, J. M. *J. Chem. Phys.* **2010**, *132*, 1251021-1−1251021-4.
(14) Rangel, N. L.; Seminario, J. A. *J. Phys. Chem. A* **2008**, *112*, 13699−13705.
(15) Wang, X.; Li, X.; Zhang, L.; Yoon, Y.; Weber, P. K.; Wang, H.; Guo, J.; Dai, H. *Science* **2009**, *324*, 768−771.
(16) Lahiri, J.; Lin, Y.; Bozkurt, P.; Oleynik, I. I.; Batzill, M. *Nat. Nanotechnol.* **2010**, *5*, 326−329.
(17) Tapaszto, L.; Dobrik, G.; Nemes-Incze, P.; Vertesy, G.; Lambin, P.; Biro, L. P. *Phys. Rev. B* **2008**, *78*, 233407-1−233407-4.
(18) Neubeck, S.; Freitag, F.; Yang, R.; Novoselov, K. S. *Phys. Status Solidi B* **2010**, *247*, 2904−2908.
(19) Garaj, S.; Hubbard, W.; Golovchenko, J. A. *Appl. Phys. Lett.* **2010**, *97*, 183103-1−183103-3.
(20) Seminario, J. M.; Yan, L.; Ma, Y. *Proc. IEEE* **2005**, *93*, 1753−1764.
(21) Plimpton, S. *J. Comput. Phys.* **1995**, *117*, 1−19.
(22) Tersoff, J. *Phys. Rev. B* **1988**, *37*, 6991−7000.
(23) Tersoff, J. *Phys. Rev. B* **1989**, *39*, 5566−5568.
(24) Tersoff, J. *Phys. Rev. Lett.* **1988**, *61*, 2879−2882.
(25) Tersoff, J. *Phys. Rev. B* **1988**, *38*, 9902−9905.
(26) Ziegler, J. F.; Biersack, J. P.; Littmark, U. *Stopping and Ranges of Ions in Matter*; Pergamon Press: New York, 1985; Vol. *1*.
(27) Lehtinen, O.; Kotakoski, J.; Krasheninnikov, A. V.; Tolvanen, A.; Nordlund, K.; Keinonen, J. *Phys. Rev. B* **2010**, *81*, 153401-1−153401-4.
(28) Eckstein, W.; Hackel, S.; Heinemann, D.; Fricke, B. *Z. Phys. D: At., Mol. Clusters* **1992**, *24*, 171−176.
(29) Nordlund, K.; Runeberg, N.; Sundholm, D. *Nucl. Instrum. Methods Phys. Res., Sect. B* **1997**, *132*, 45−54.
(30) Berendsen, H. J. C.; Postma, J. P. M; van Gunsteren, W. F.; DiNola, A.; Haak, J. R. *J. Chem. Phys.* **1984**, *81*, 3684−3690.
(31) Ito, A.; Nakamura, H.; Takayama, A. *J. Phys. Soc. Jpn.* **2008**, *77*, 114602-1−114602-13.
(32) Floro, J. A.; Rossnagel, S. M.; Robinson, R. S. *J. Vac. Sci. Technol., A* **1983**, *1*, 1398−1402.
(33) Perdew, J. P.; Wang, Y. *Phys. Rev. B* **1992**, *45*, 13244−13249.
(34) Perdew, J. P.; Chevary, J. A.; Vosko, S. H.; Jackson, K. A.; Pederson, M. R.; Singh, D. J.; Fiolhais, C. *Phys. Rev. B* **1992**, *46*, 6671−6687.
(35) Hariharan, P. C.; Pople, J. A. *Chem. Phys. Lett.* **1972**, *16*, 217−219.
(36) Seminario, J. M.; Concha, M. C.; Politzer, P. *J. Chem. Phys.* **1995**, *102*, 8281−8282.
(37) Seminario, J. M.; Concha, M. C.; Murray, J. S.; Politzer, P. *Chem. Phys. Lett.* **1994**, *222*, 25−32.
(38) Politzer, P.; Seminario, J.; Bolduc, P. *Chem. Phys. Lett.* **1989**, *158*, 463−469.
(39) Murray, J.; Redfern, P.; Seminario, J.; Politzer, P. *J. Phys. Chem.* **1990**, *94*, 2320−2323.
(40) Murray, J. S.; Seminario, J. M.; Politzer, P. *Int. J. Quantum Chem.* **1994**, *49*, 575−579.
(41) Hashimoto, A.; Suenaga, K.; Gloter, A.; Urita, K.; Iijima, S. *Nature* **2004**, *430*, 870−873.